# Electronic Supplementary Information

## 3D self-supported Ni nanoparticle@N-doped carbon nanotubes anchored on NiMoN pillars for hydrogen evolution reaction with high activity and anti-oxidation ability

Yi Gong,‡[a] Linan Wang,‡[a] Hailang Xion,[b] Mingfei Shao,[c] Lidong Xu,[a] Ao Xie,[a] Shuxian Zhuang,[a] Yang Tang,*[a] Xiaojin Yang,[b] Yongmei Chen,[a] and Pingyu Wan,*[a]

[a] Institute of Applied Electrochemistry, Beijing University of Chemical Technology, 100029 Beijing, PR China.

Email: tangyang@mail.buct.edu.cn, pywan@mail.buct.edu.cn

[b] National Fundamental Research Laboratory of New Hazardous Chemicals Assessment & Accident Analysis, Beijing University of Chemical Technology, 100029 Beijing, PR China.

[c] State Key Laboratory of Chemical Resource Engineering, Beijing University of Chemical Technology, 100029 Beijing, PR China

‡ These authors contributed equally to this work.

# 1. Experimental Section

### Materials and chemicals

Nickel nitrate hexahydrate ($Ni(NO_3)_2 \cdot 6H_2O$), ammonium heptamolybdate tetrahydrate ($(NH_4)_6Mo_7O_{24} \cdot 4H_2O$) were purchased from Aladdin Chemical Reagent Co. Ltd. Nickel foam (NF, thickness 1.5 mm, 110 PPI) was purchased from LiZhiYuan Electronic Materials Co. Ltd. Dicyandiamide, potassium hydroxide, ethyl alcohol, hydrochloric acid and sulphuric acid were purchased from Beijing Chemical Reagent Co. Ltd. Commercial Pt/C (20 wt %) was purchased from Alfa Aesar Chemical Reagent Co. Ltd.

### Synthesis of Ni@NCNT/NiMoN/NF

The synthesis of the hierarchical Ni@NCNT/NiMoN/NF electrocatalyst involves two steps. In this work, the nickel foam (NF) was first cut into pieces of $3 \times 5$ $cm^2$ and successively pre-treated in ethanol, 1 M HCl and deionized water under ultrasonic condition to remove the impurities and oxidation film, and then dried naturally. First, the cleaned NF was placed in a Teflon-lined stainless steel autoclave which contained 0.04 M $Ni(NO_3)_2 \cdot 6H_2O$ and 0.01 M $(NH_4)_6Mo_7O_{24} \cdot 4H_2O$ and 80 mL deionized water. The growth of $NiMoO_4$ pillars was performed with heating the autoclave at 150 °C for 6 h in an electric oven. After natural cooling to room temperature, the resulting light yellow $NiMoO_4$ precursor (denoted as $NiMoO_4$/NF) was taken out and washed with deionized water for several times and dried in a vacuum oven at 80 °C for 12 h. Second, the $NiMoO_4$/NF was calcinated with dicyandiamide (denoted as DCDA) from room temperature to 500 °C with a heating rate of 5 °C $min^{-1}$ and kept for 1 h, followed by increasing the temperature to 800 °C at a heating rate of 30 °C $min^{-1}$ and keeping for 2 h in a $H_2$/Ar (5:95) atmosphere. After calcination at high temperature, the initial yellow-colored $NiMoO_4$/NF samples all turned into black, and the product was denoted as Ni@NCNT/NiMoN-8 with a loading weight of ~ 41.3 mg

$cm^{-2}$, where 8 represented the pyrolysis temperature of 800 °C. The samples named Ni@NCNT/NiMoN-7 and Ni@NCNT/NiMoN-9 were prepared in the same way except for the second heat treatment at 700 °C and 900 °C, respectively. The loading

**Synthesis of $Ni_4Mo/MoO_2$/NF**

The $Ni_4Mo/MoO_2$/NF electrode was synthesized under a similar condition of Ni@NCNT/NiMoN-8 but without the absence of DCDA in pyrolysis process.

**Synthesis of Pt/C electrode**

The Pt/C electrode was prepared by homogeneously dispersing 10 mg commercial Pt/C (20 wt%) in 1200 μL dimethyl formamide and 800 μL of 0.5 wt% Nafion solution, and then loading the as-prepared solution with 400 μL $cm^{-2}$ on the Ni foam. Therefore, the weight density of Pt/C on Ni foam is 2 mg $cm^{-2}$.

**Characterizations**

Scanning electron microscopy (SEM) and Energy dispersive X-ray spectroscopy (EDS) elemental mapping characterization were carried out with a Zeiss SUPRA 55 electron microscopy. The high angle annular dark-field scanning transmission electron microscopy (HAADF-STEM) with EDS elemental mapping and the high-resolution transmission electron microscopy (HRTEM) including SAED were performed on a Tecnai G2 F30 microscope with an acceleration voltage of 200 kV. The X-ray diffraction (XRD) patterns were recorded on a Bruker D8-Advance diffractometer with Cu Kα radiation (hυ = 1486.6 eV) with a scanning rate of 5° $min^{-1}$. The Raman spectra were obtained on a Renishaw in Via Reflex with the 532 nm laser. The X-ray photoelectron spectroscopy (XPS) spectra were collected using an ESCALAB250X with a monochromated Al Kα 150 W X-ray source.

**Electrochemical Measurements**

The electrocatalytic HER performance of the samples were evaluated on a CH Instruments electrochemical workstation (CHI 660E) with a three-electrode setup, in which the prepared electrodes (Ni@NCNT/NiMoN-7, 8 and 9 , $1\times1$ $cm^2$) were used as the working electrodes, a $RuO_2$/Ti electrode as the counter electrode and a saturated calomel electrode (SCE) as the reference electrode. Before the electrochemical measurements, the electrolyte (1 M KOH or 0.5 M $H_2SO_4$) was purged with Ar for 30 min to remove the dissolved gases completely. In all measurements, the potentials were calculated with respect to reversible hydrogen electrode (RHE) based on the following equation: $E_{(RHE)} = E_{(SCE)} + 0.05916\times pH + 0.2412$ V, and the ohmic potential drop on the electrolyte resistance has been subtracted according to the equation: $E_{compensated} = E_{measured} - i\times R_s$ ($R_s$ is determined by EIS). Pure NF, $NiMoO_4$/NF, and commercial 20 wt% Pt/C catalyst with a weight density of 2.0 mg $cm^{-2}$ were also measured for comparison.

The linear sweep voltammetry (LSV) tests were conducted at the scan rate of 1 mV $s^{-1}$ after 5 cycles of cyclic voltammetry (CV) tests to stabilize the current. Tafel plots were derived from LSV curves. Electrochemical impedance spectroscopy (EIS) spectra were recorded with operating overpotential set at -0.1 V (vs. RHE), and frequency ranged from 100 000 to 0.01 Hz with an amplitude of 5 mV. The double-layer capacitance ($C_{dl}$), which was proportional to the ECSA, was measured by a typical cyclic voltammetry (CV) test at different scan rates from 5 to 30 mV $s^{-1}$ in the potential range from 0.02 to 0.19 V. The durability test was carried out at a constant current density for 24 h, during which the overpotential variation with time was recorded. The scale-up overall water splitting measurement was carried out in a standard two-electrode system by using Ni@NCNT/NiMoN-8 as both anode and cathode.

**DFT Calculations**

In the present work, the density functional theory (DFT) calculations were

performed by using a plane wave implementation[1] with the CASTEP module of Material Studio 6.0. The Perdew-Burke-Ernzerhof (PBE) functional in generalized gradient approximation (GGA) was used to describe the electron exchange and correlation.[2] The transition metals (Ni and Mo) were treated with the spin-polarized DFT + U theory in this work. The values of U - J (Ueff) were 3.80 eV for Ni[3] and 3.50 eV for Mo,[4] respectively. The core electrons were performed with the ultrasoft pseudo-potentials to improve transferability.[5] The energy cut-off of 400 eV was applied for the plane wave truncation.[6] The value of self-consistent field (SCF) tolerance was $1 \times 10^{-6}$ eV/atom.[7] All geometry optimizations of structures were based on the following three points: (a) an energy tolerance of $2 \times 10^{-5}$ eV/atom, (b) a max force of 0.05 eV/Å and (c) a max displacement of 0.002 Å. In addition, the plains of crystal surfaces were selected and calculated based on the results of HRTEM.[8]

The primitive model for Ni was modeled with the space group of $fm\bar{3}m$, indicating that $\alpha = \beta = \gamma = 90^{o}$. The other three lattice parameters, *a*, *b*, and *c*, were accordance with the XRD data. The Ni(111) surface was constructed by cleaving optimized bulk Ni in a five-layers slab.[9] The two top-most layers of Ni were fully relaxed during the optimization of the overall adsorption structure, indicating that the other layers were immobilized.[10] The lattice parameter of the Ni(111) surface is well known to be 2.492 Å × 2.492 Å.[11] The size of supercell of 4 × 4, 9.968 Å × 9.968 Å, was used for calculations of Ni(111), whereas the lattice parameter of the orthorhombic 4 × 2 supercell of graphene, 9.840 Å × 8.520 Å.[12] To make up for such a lattice mismatch of the Ni(111) surface and the graphene layer, we utilized the surface lattice constant of 9.968 Å × 8.946 Å for the Ni(111)@C heterostructure. It's worth noting that this does not transform the structures of both the graphene and the Ni(111) layer. With this constant, N-doped graphene layer was put on the surface of Ni(111) to form Ni(111)@NC heterostructure. The Brillouin zone was 3 × 3 × 1 k-points sampled with Monkhorst-Pack Scheme.[13] 18 Å of vacuum was performed in the direction of z- between periodically repeated images to avoid the repeated interaction.[13, 14]

The primitive model for MoN was performed with the space group of $p\bar{6}m2$,

indicating that $\alpha = \beta = 90^{o}$ , $\gamma = 120^{o}$ . The other caculated lattice constants, *a*, *b*, and *c*, were referred to the XRD patterns. The supercell of MoN was 3 × 3 × 1 in the directions of a-, b-, c-. With this model of supercell, one Mo atom was randomly replaced by Ni atom, which formed the model of NiMoN. Its (101) surface formed the surface of the NiMoN system. The lattice parameter of the 3 × 3 cell of NiMoN(101) surface was 9.116 Å × 8.658 Å, while the lattice constant of the orthorhombic 4 × 2 supercell of graphene, 9.840 Å × 8.520 Å. To compensate the mismatching lattice constant between the NiMoN(101) surface and the graphene layer, the surface lattice constant of C/NiMoN(101) heterostructure, 9.116 Å × 8.589 Å, was adopted. With this constant, N-doped graphene layer was put on the surface of NiMoN(101) to form NC/NiMoN(101) heterostructure. The Brillouin zone and vacuum thickness are 3 × 3 × 1 and 18 Å, respectively.

In the above-mentioned two systems, we adsorbed H* and $H_2O$ molecule to calculate their adsorption energy. The hydrogen adsorption energy ($\Delta E_{H*}$) and the water adsorption energy ($\Delta E_{H_2O}$) were respectively defined as:

$$\Delta E_{H*} = E_{slab+H*} - E_{slab} - \frac{1}{2}E_{H_2}$$

$$\Delta E_{H_2O} = E_{slab+H_2O} - E_{slab} - E_{H_2O}$$

Where $E_{slab+H_2O}$ and $E_{slab+H*}$ are the total energy of the slab with a $H_2O$ molecule and an atomic hydrogen, respectively, $E_{slab}$ is the total energy of the slab, $E_{H_2O}$ and $E_{H_2}$ are the energy of a gas phase $H_2O$ molecule and a gas phase $H_2$ molecule, respectively. The free energy of hydrogen adsorption was calculated as:

$$\Delta G_{H*} = \Delta E_{H*} - \Delta E_{ZPE} - T\Delta S_{H*}$$

where $\Delta E_{H*}$ is the adsorption energy of an atomic hydrogen on the slab, $\Delta E_{ZPE}$ and $\Delta S_{H*}$ are zero point energy change and entropy change of H* adsorption, respectively. The entropy of absorbed state hydrogen is so small and negligible.[15, 16] Herein, $\Delta S_{H*}$ can be corrected as -1/2 $S_{H_2}$, where $S_{H_2}$ is the entropy of $H_2$ in the gas phase at standard conditions. Therefore, with overall values, the Gibbs free energy can be calculated as

$\Delta G_{H*} = \Delta E_{H*} + 0.24$ eV, as similarly reported by Nørskov et al.[17]

## 2. Supplementary Figures and Tables

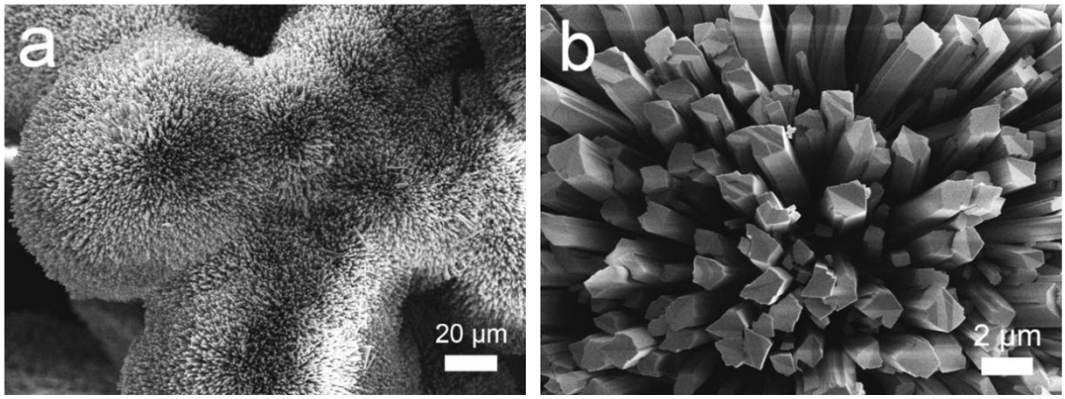


**Fig. S1** Typical SEM images of $NiMoO_4$/NF.

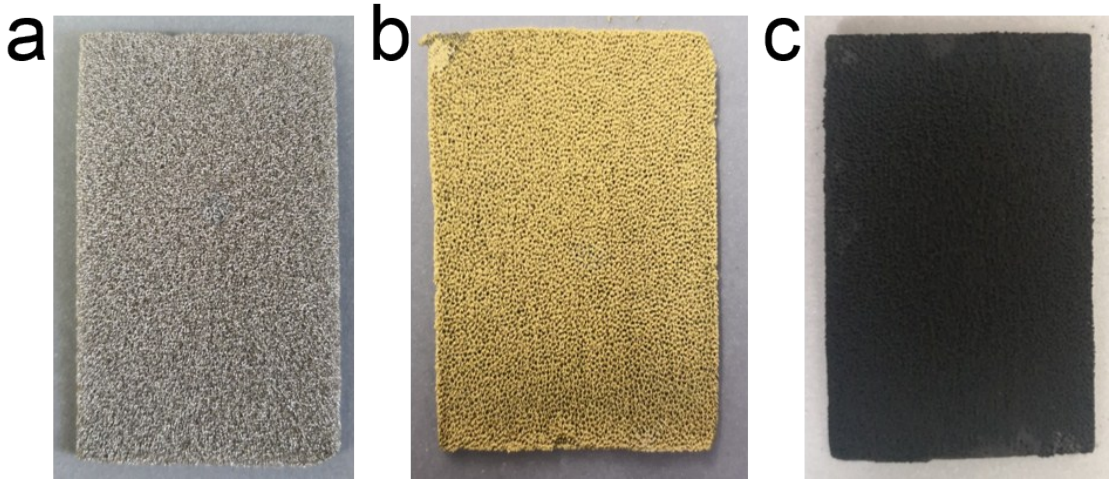


**Fig. S2** Photographs of (a) NF, (b) $NiMoO_4$/NF and (c) Ni@NCNT/NiMoN-8.

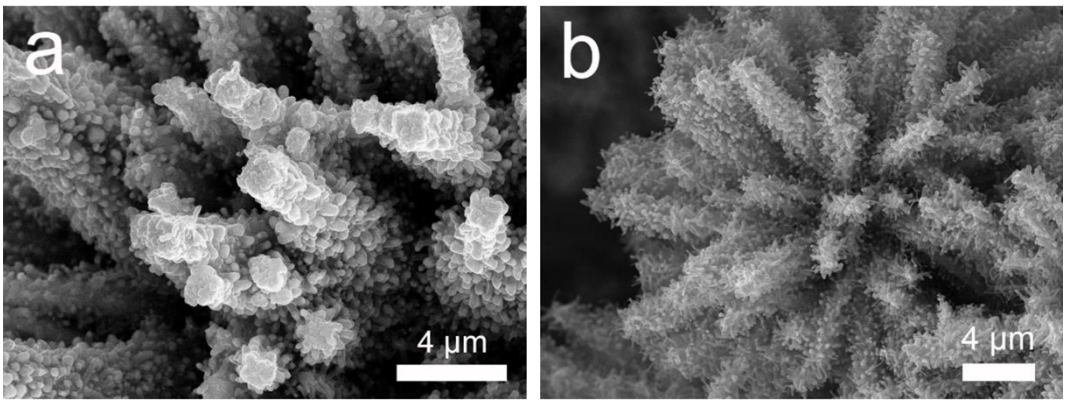


**Fig. S3** Typical SEM images of (a) Ni@NCNT/NiMoN-7 and (b)

Ni@NCNT/NiMoN-9.

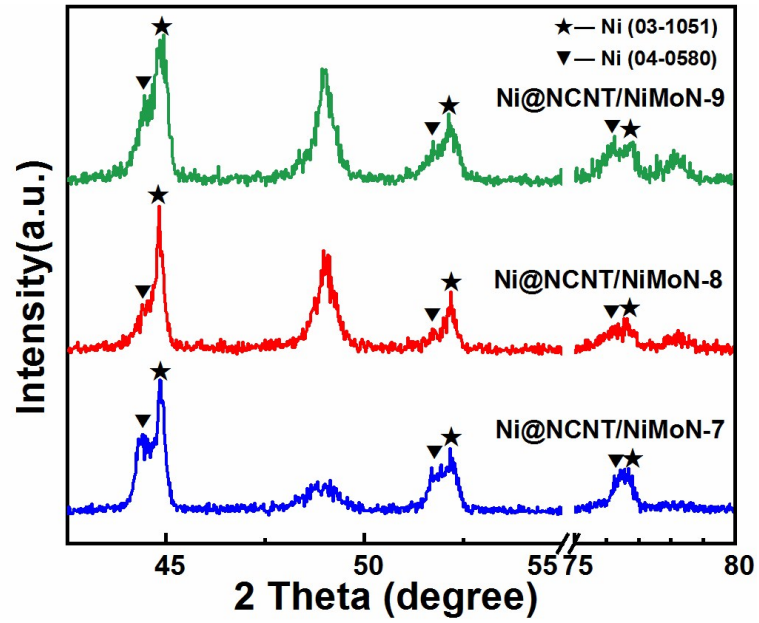


**Fig. S4** The partial enlarged details for Ni (03-1051) and Ni (04-0850) of Ni@NCNT/NiMoN-7,8,9.

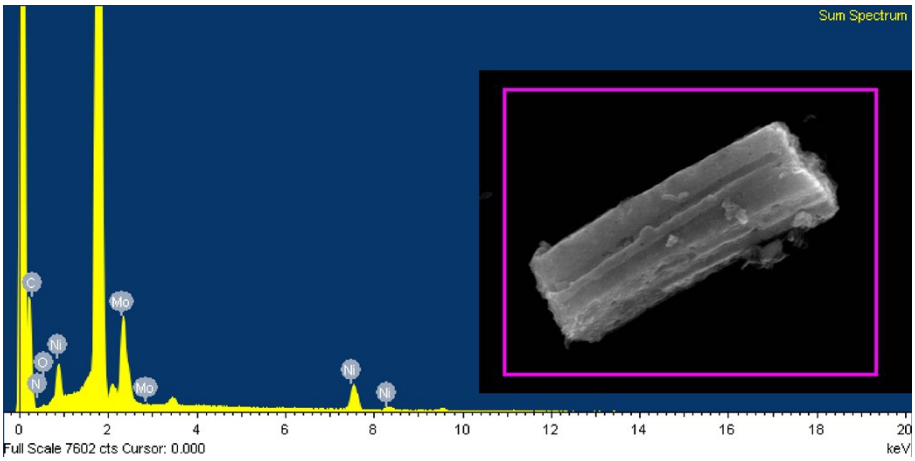


**Fig. S5** EDS spectrum and element analysis of NiMoN MP.

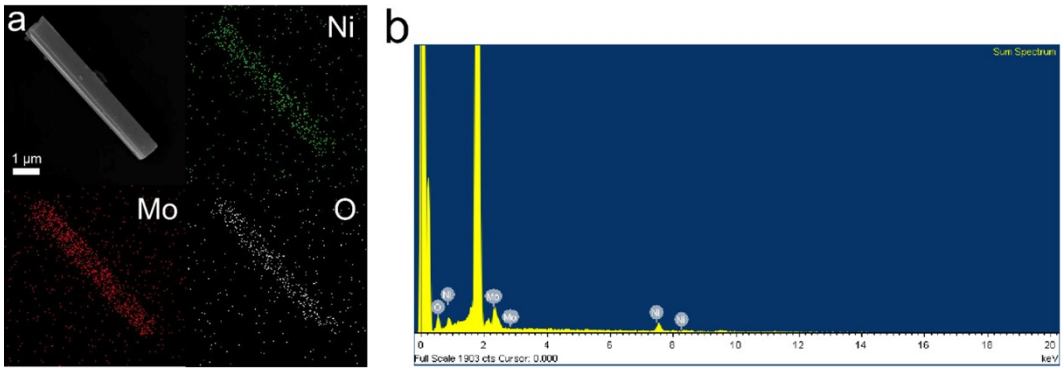


**Fig. S6** (a) EDS mapping images and (b) EDS spectrum of $NiMoO_4$ pillar peeled off from NF.

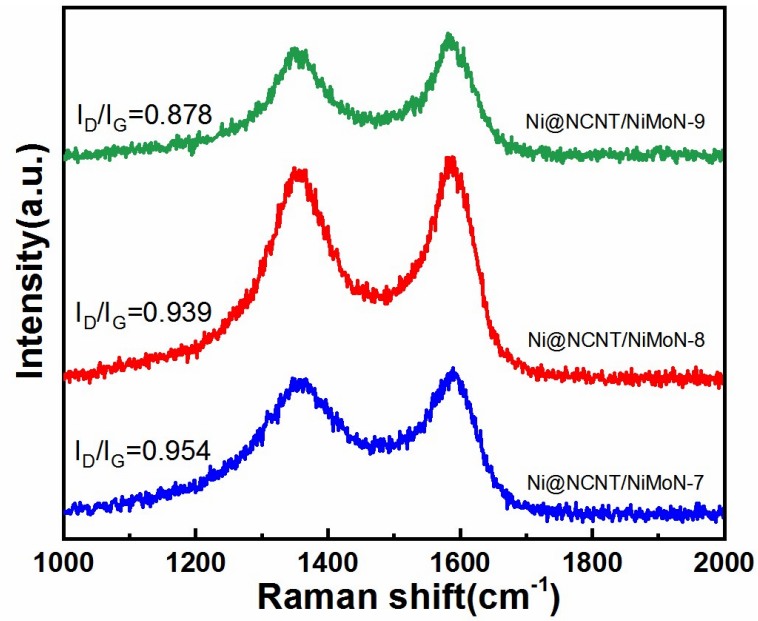


**Fig. S7** Raman spectra of Ni@NCNT/NiMoN after being calcined at different temperatures.

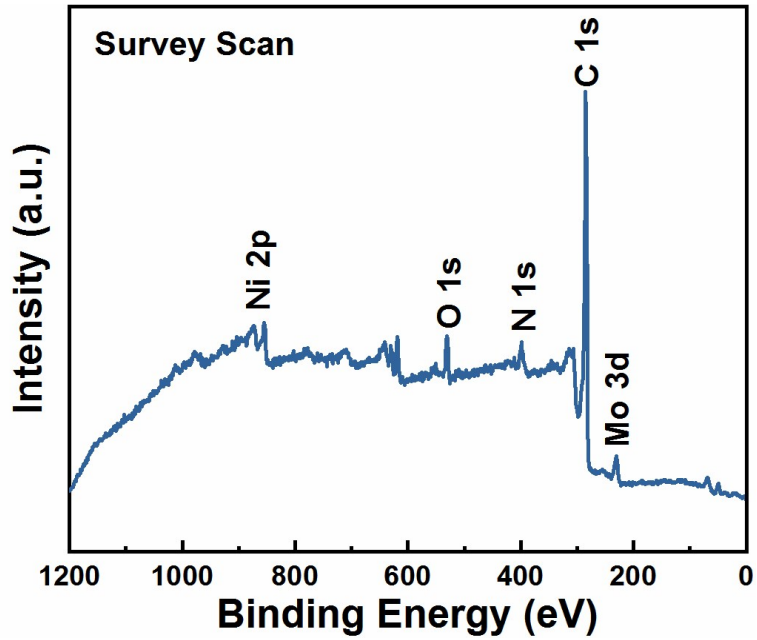


**Fig. S8** XPS spectrum of Ni@NCNT/NiMoN-8.

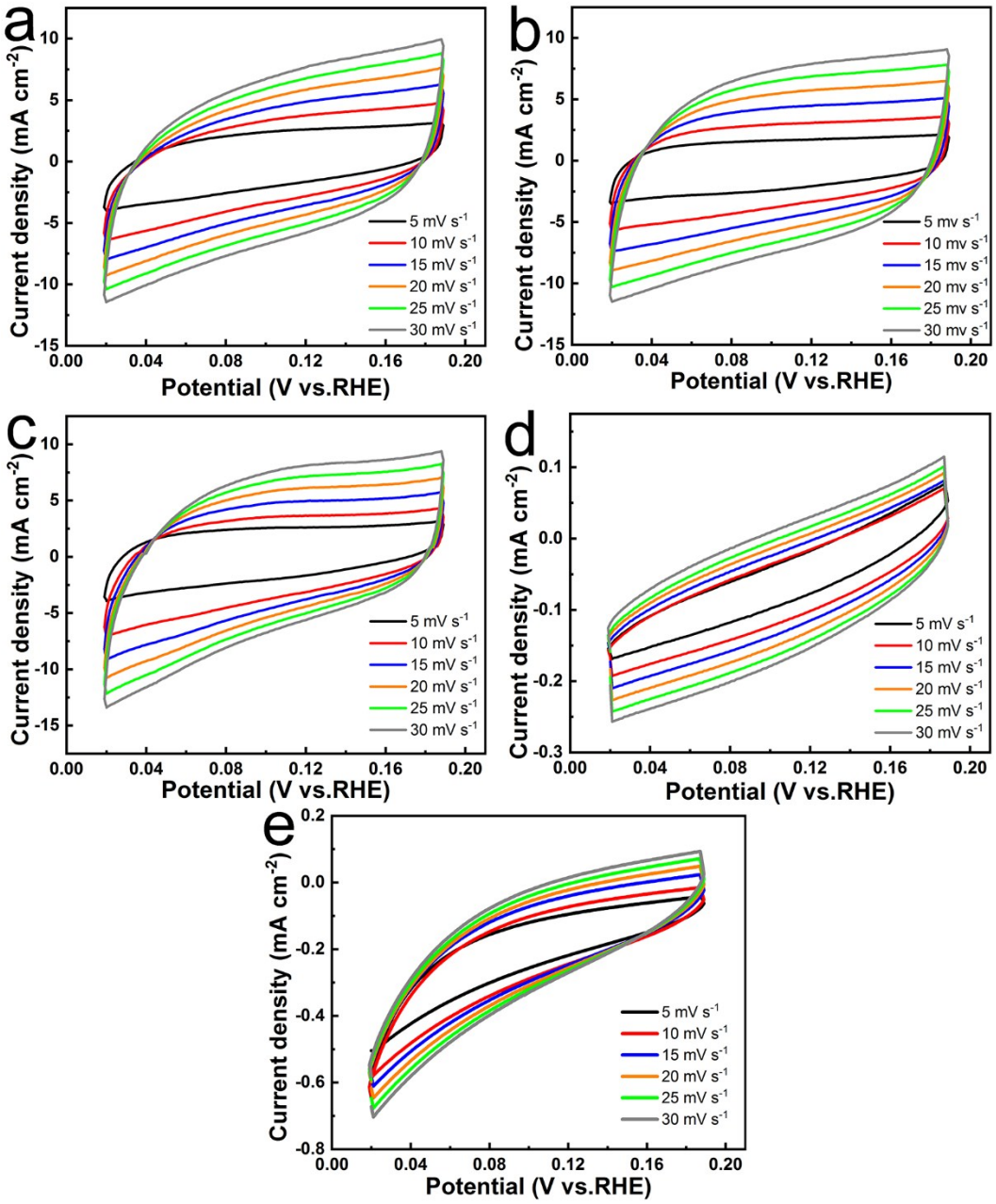


**Fig. S9** CV curves of (a) Ni@NCNT/NiMoN-7, (b) Ni@NCNT/NiMoN-8, (c) Ni@NCNT/NiMoN-9, (d) NF and (e) $NiMoO_4$/NF at different scan rates.

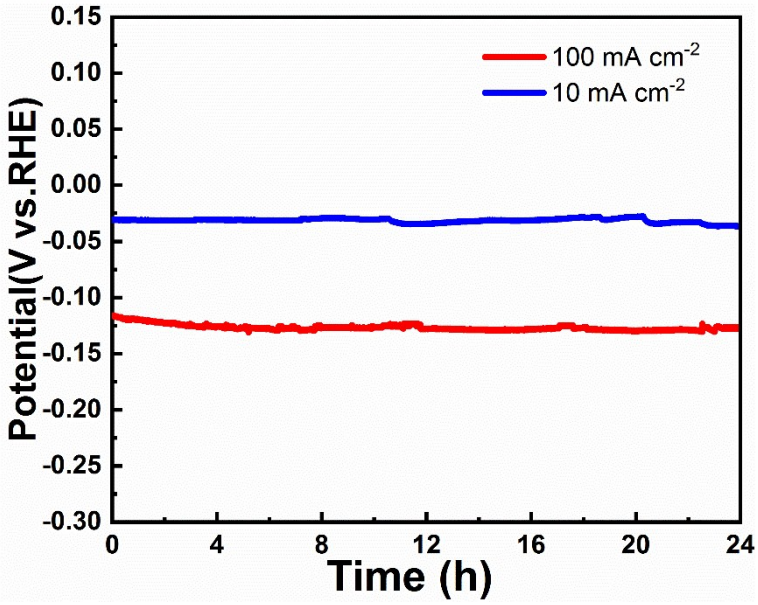


**Fig. S10** Chronopotentiometric curves of Ni@NCNT/NiMoN-8 at constant current densities of 10 and 100 mA $cm^{-2}$ in 1 M KOH.

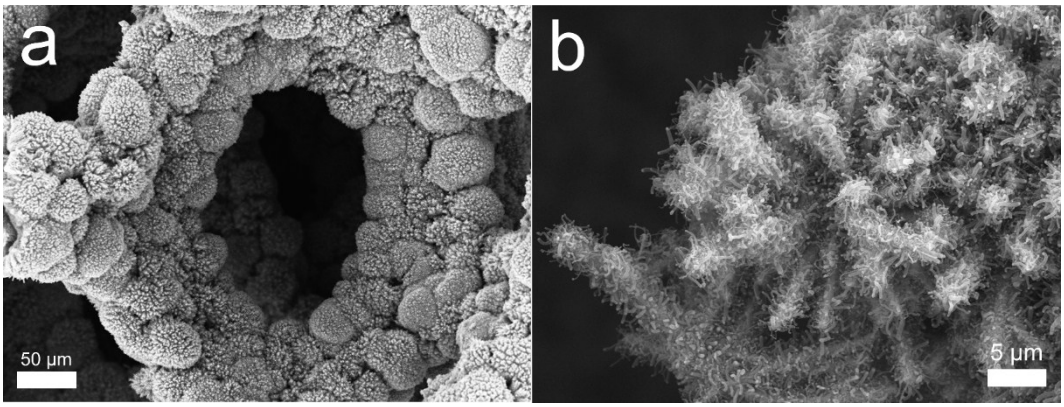


**Fig. S11** SEM images of Ni@NCNT/NiMoN-8 after 48 h durability test for HER at different scales.

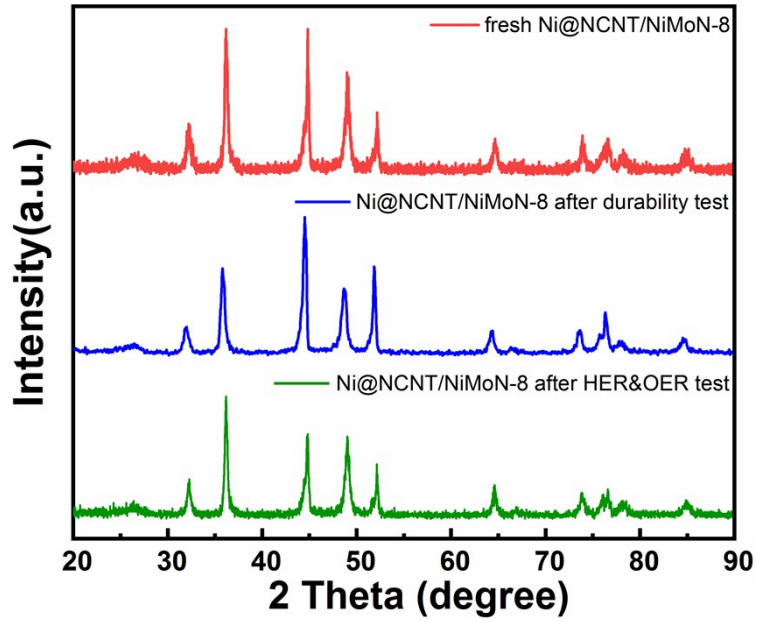


**Fig. S12** XRD patterns of fresh Ni@NCNT/NiMoN, Ni@NCNT/NiMoN after durability test and Ni@NCNT/NiMoN after HER&OER cycles.

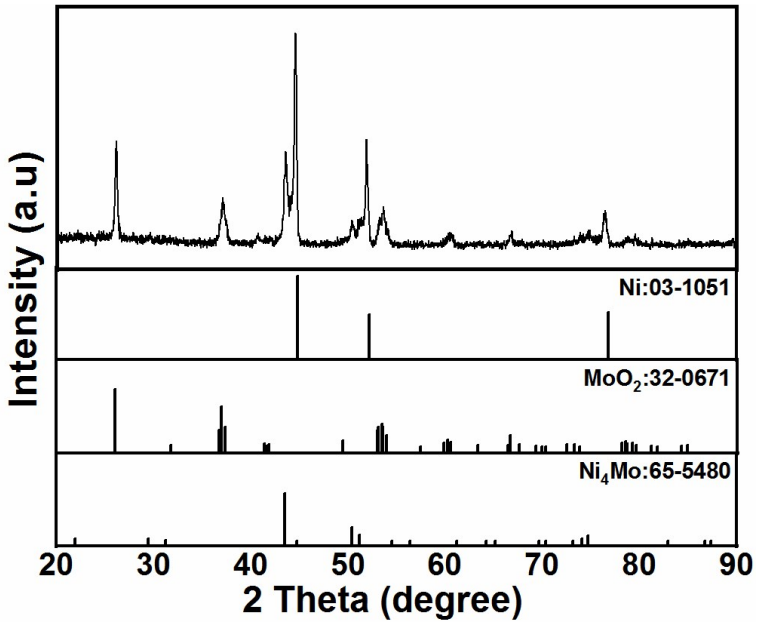


**Fig. S13** XRD patterns for $Ni_4Mo/MoO_2$/NF.

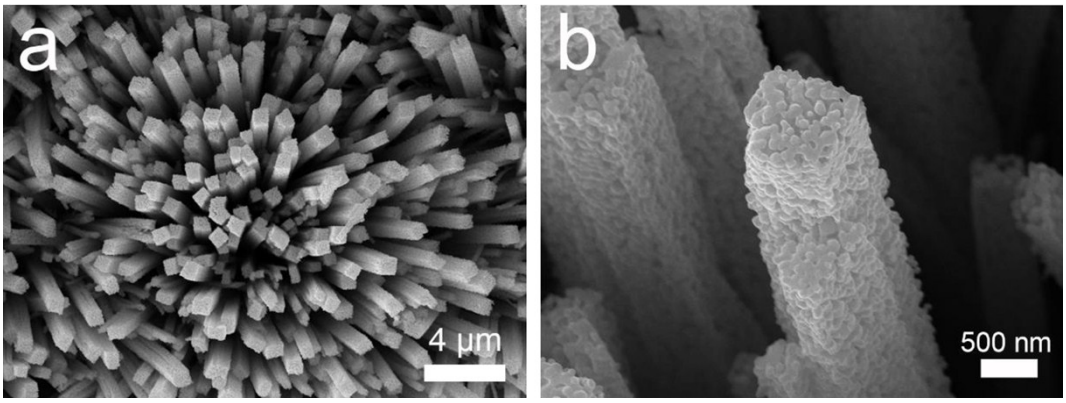


**Fig. S14** The SEM images of $Ni_4Mo/MoO_2$/NF.

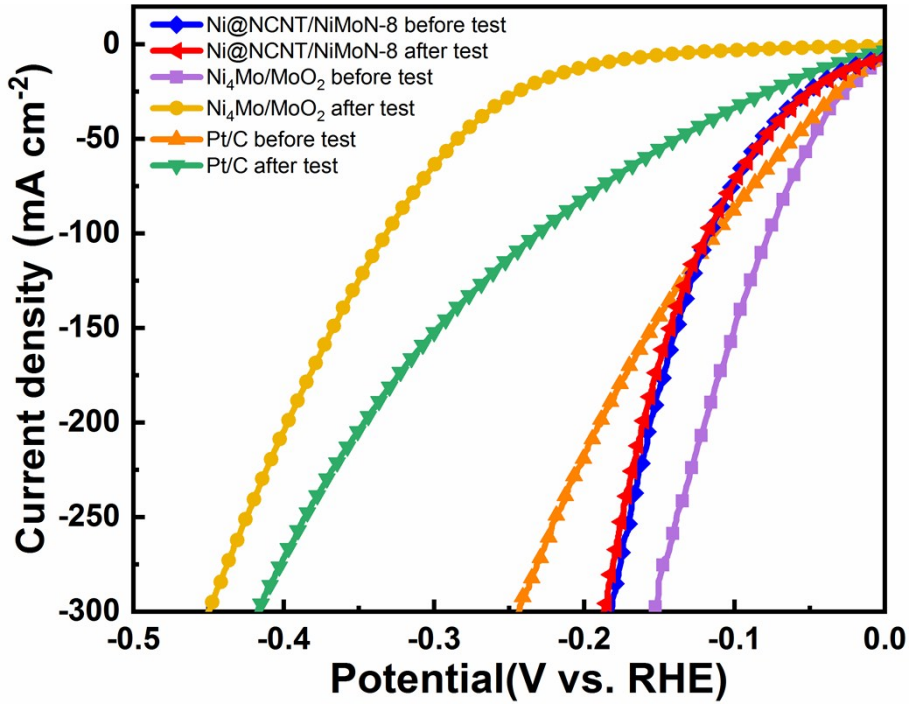


**Fig. S15** Polarization curves of Ni@NCNT/NiMoN-8, $Ni_4Mo/MoO_2$/NF and Pt/C for HER before and after HER&OER cycles.

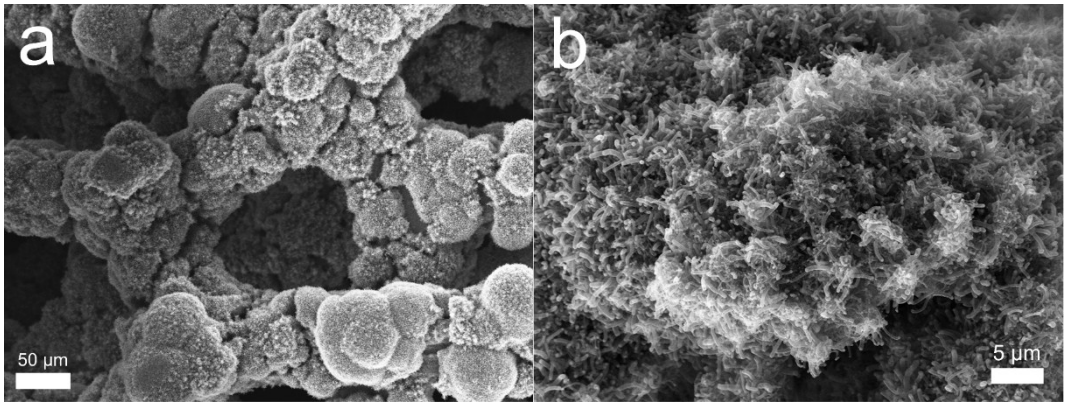


**Fig. S16** SEM images of Ni@NCNT/NiMoN-8 after HER&OER cycles at different scales.

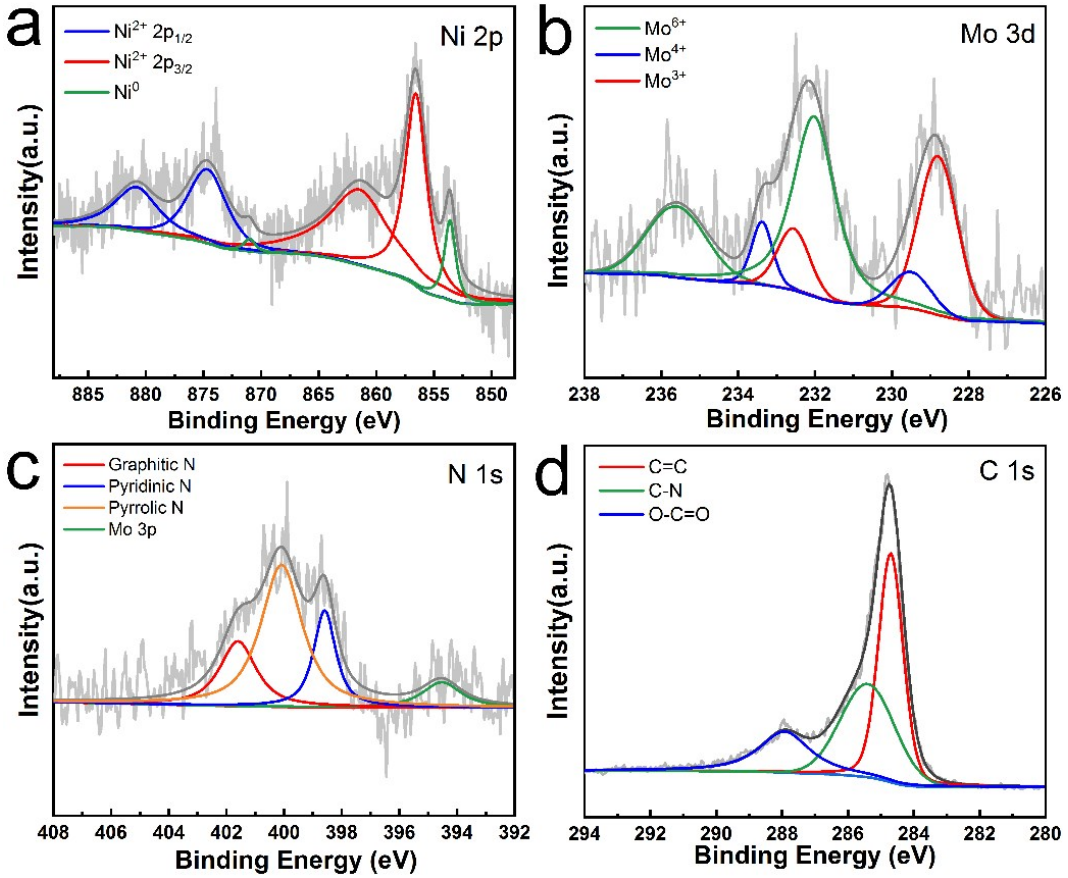


**Fig. S17** XPS spectra of (a) Ni 2p region, (b) Mo 3d region, (c) N 1s-Mo 3p region and (d) C 1s region for Ni@NCNT/NiMoN-8 after HER&OER cycles.

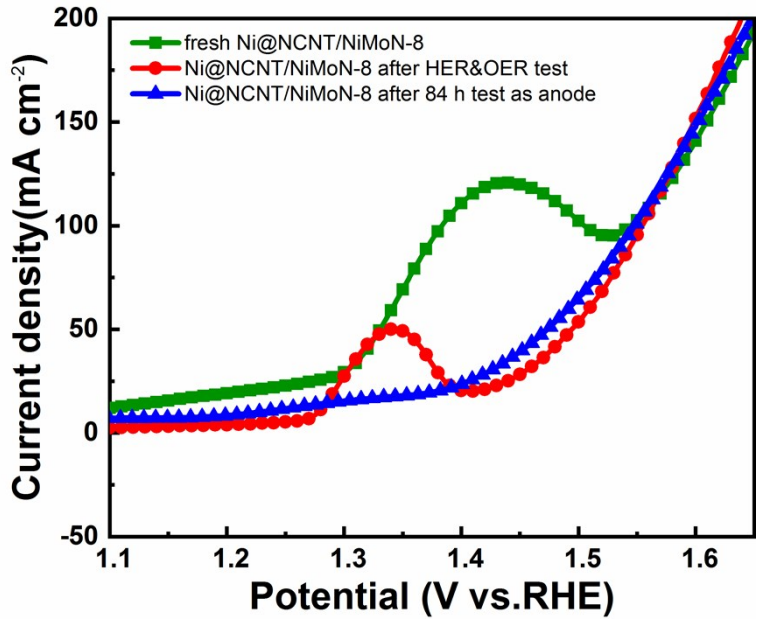


**Fig. S18** LSV curves for OER of fresh Ni@NCNT/NiMoN-8, Ni@NCNT/NiMoN-8 after HER&OER cycles test and Ni@NCNT/NiMoN-8 after 84 h water splitting test as anode.

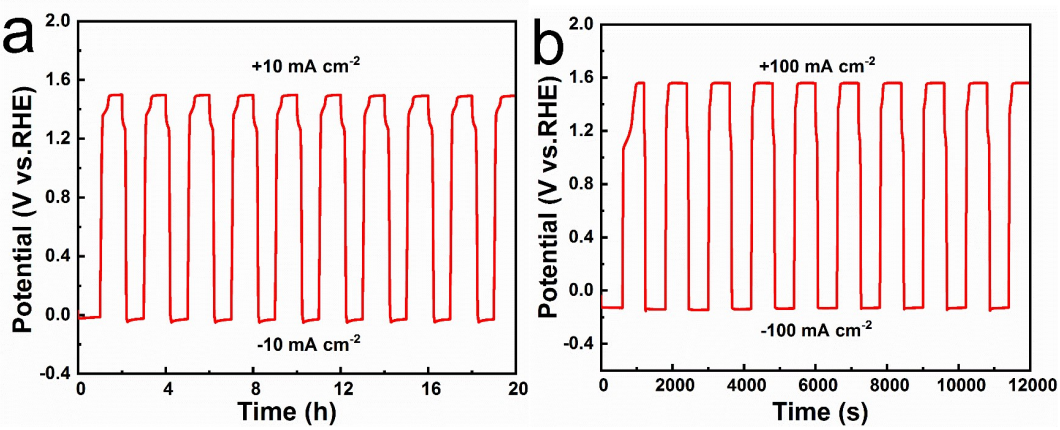


**Fig. S19** HER&OER cycles chronopotentiometric curves of Ni@NCNT/NiMoN-8 at current densities of (a) ± 10 mA $cm^{-2}$; (b) ± 100 mA $cm^{-2}$.

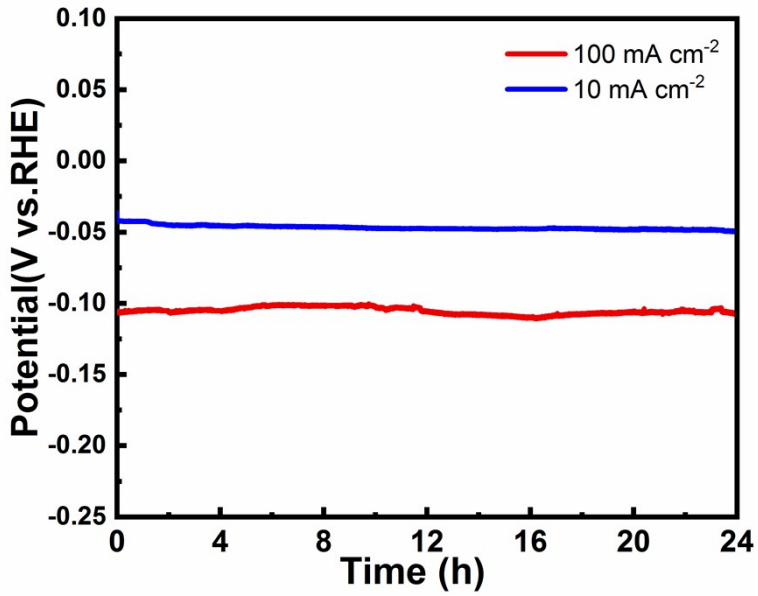


**Fig. S20** Chronopotentiometric curves of Ni@NCNT/NiMoN-8 at constant current densities of 10 and 100 mA $cm^{-2}$ in 0.5 M $H_2SO_4$.

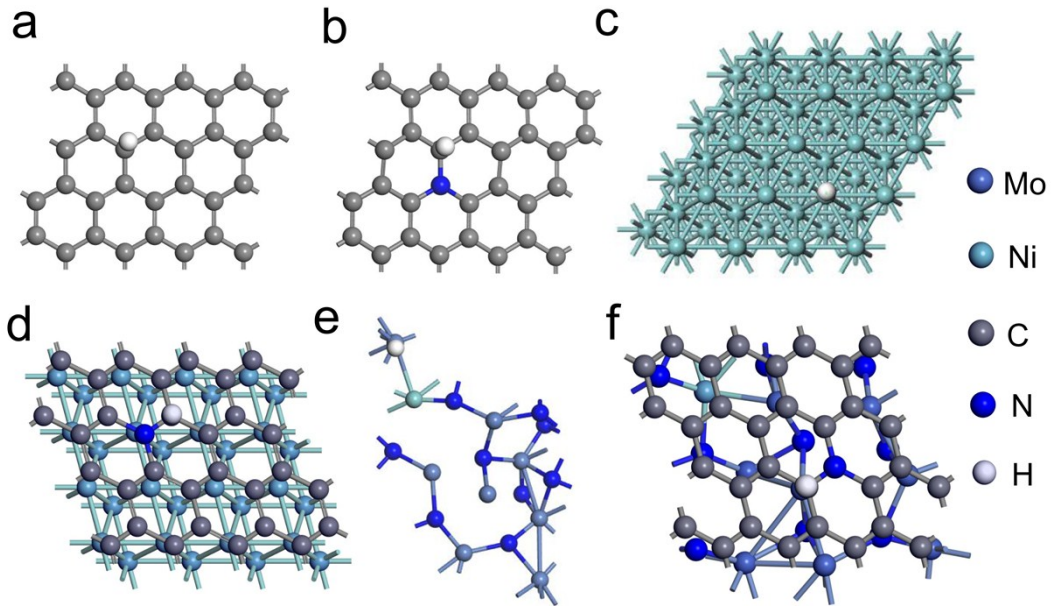


**Fig. S21** Top view of the theoretical models of H* adsorption on the different catalysts (a) graphene, (b) N-doped graphene, (c) Ni(111), (d) Ni(111)@NC heterostructure, (e) NiMoN(101) and (f) NC/NiMoN(101) heterostructure. The color for each element is labeled.

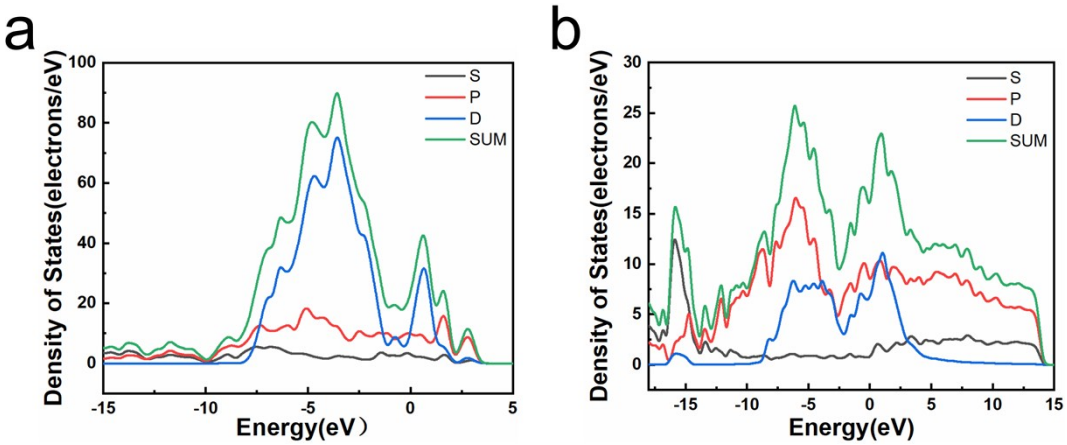


**Fig. S22** The calculated total and partial electronic density of states (TDOS and PDOS) for (a) Ni(111)@NC heterostructure and (b) NC/NiMoN(101) heterostructure.

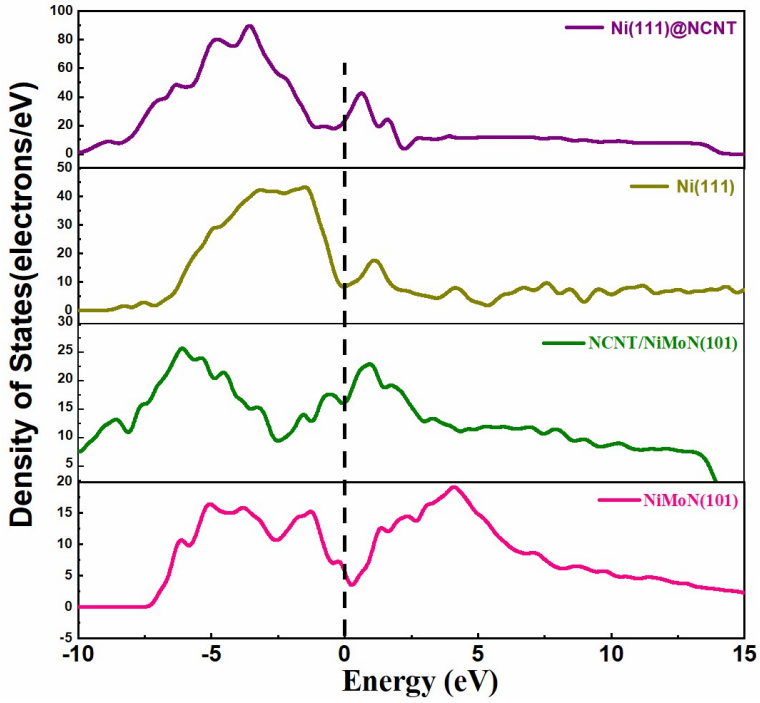


**Fig. S23** The calculated TDOS for NiMoN(101), NC/NiMoN(101) heterostructure, Ni(111) and Ni(111)@NC heterostructure. The black dashed line denotes the position of the Fermi level (0 eV).

**Table S1** Elementary composition of a Ni nanoparticle.

| Element | Weight% | Atomic% | Uncert. % | Detector Correction | k-Factor |
|---|---|---|---|---|---|
| Ni (K) | 97.82 | 98.66 | 0.54 | 0.99 | 1.453 |
| Mo (L) | 2.17 | 1.33 | 0.23 | 0.98 | 4.047 |

**Table S2 Elementary composition of a NiMoN** pillar**.**

| Element | Weight% | Atomic% |
|---|---|---|
| C (K) | 38.19 | 61.98 |
| N (K) | 17.33 | 24.12 |
| O (K) | 3.41 | 4.16 |
| Ni (K) | 10.91 | 3.62 |
| Mo (L) | 30.16 | 6.13 |
| Totals | 100.00 | 100.00 |

**Table S3** Elementary composition of a $NiMoO_4$ pillar.

| Element | Weight% | Atomic% |
|---|---|---|
| O (K) | 48.61 | 82.53 |
| Ni (K) | 16.25 | 7.52 |
| Mo (L) | 35.14 | 9.95 |
| Totals | 100.00 | 100.00 |

**Table S4** Comparison of HER activity of Ni@NCNT/NiMoN-8 electrode with recently reported catalysts in 1.0 M KOH.

| **Catalysts** | **$\eta_{10}$ (mV vs RHE)** | **$\eta_{100}$ (mV vs RHE)** | **Ref.** |
|---|---|---|---|
| Ni@NCNT/NiMoN-8 | 15 | 117 | This work |
| N-$NiMoO_4$/$NiS_2$ | 57 | 267 | [18] |
| NiMoP NSs@MCNTs | 135 | 300 | [19] |
| $Ni_{foam}$@Ni-$Ni_{0.2}Mo_{0.8}N$ | 15 | - | [20] |
| NiMoN-550 nanotubes | 89 | - | [21] |
| $Ni_2P$/$MoO_2$@$MoS_2$ | 159 | - | [22] |
| NiMoN/NF-450 | 22 | - | [23] |
| $Ni_3N$-NiMoN | 31 | 210 | [7] |
| NiMo HNRs/TiM | 92 | 200 | [24] |
| Ni/$Mo_2C$-PC | 179 | - | [25] |
| Ni-Mo Ms/Cu | 63 (20 mA $cm^{-2}$) | - | [26] |
| $Ni(PO_3)_2$-$MoO_3$/NF | 86 | 205 | [27] |
| P-$NiMo_4N_5$@Ni | 118 | - | [28] |
| N,P-$Mo_xC$ NF | 135 | - | [29] |
| $NiS_2$/$MoS_2$ HNW. | 204 | - | [30] |
| $NiMo_3S_4$ | 257 | - | [31] |
| NiMo NWs/Ni | 30 | 125 | [32] |
| MoP/C | 49 | - | [33] |
| CoP/NiCoP/NC | 75 | | [34] |
| NC–NiCu–NiCuN | 93 | 149 | [35] |
| Cu@NiFe LDH | 116 | 192 | [36] |
| $NiCo_2P_x$ | 58 | 127 | [37] |
| $Ni_{0.89}Co_{0.11}Se_2$ MNSN/NF | 85 | - | [38] |
| Co-Ex-$MoS_2$ | 89 | - | [39] |
| N-$NiCo_2S_4$ | 41 | - | [40] |

| | | | |
|---|---|---|---|
| $NiCo_2S_4/Ni_3S_2/NF$ | 119 | 600(600 mA $cm^{-2}$) | [41] |
| FLNPC@MoP-NC/MoP-C/CC | 69 | - | [42] |
| Co/CoP@NC | 180 | - | [43] |
| $Ni_3S_2/NF$ | 164 | - | [44] |
| $Ni_3S_2/NF$-4 | 89 | 186 | [45] |
| $NiP_2$/NiO NRs | 131 | - | [46] |
| Co@N-CNTs@rGO | 108 | - | [47] |
| Co/β-$Mo_2C$@N-CNTs | 170 | - | [48] |
| NF@Ni/C-600 | 37 | 124(50 mA $cm^{-2}$) | [49] |
| L-$Mo_2C$ | 95.8 | | [50] |
| $Ni_3Fe$@N-C NT/NFs | 72 | - | [15] |
| mNC-$Mo_2C$@rGO-2 | 95 | - | [51] |
| NC@$CuCo_2N_x$/CF | 105 | - | [52] |
| $MoS_2$/CNT-700 | 86 | - | [53] |
| $NiCo_2P_2$–CNT | 48 | | [54] |
| $Co_3O_4$–$Co_4N$ | 90 | | [55] |
| FeNiOH/NF | 160 | 312 | [56] |

**Table S5** Comparison of OER activity of Ni@NCNT/NiMoN-8 electrode with recently reported catalysts in 1.0 M KOH.

| **Catalysts** | **$\eta_{10}$ (mV vs RHE)** | **$\eta_{100}$ (mV vs RHE)** | **Ref.** |
|---|---|---|---|
| Ni@NCNT/NiMoN-8 | 261 | 338 | This work |
| N-$NiMoO_4$/$NiS_2$ | 281 | 335 | [18] |
| NiMoP NSs@MCNTs | 255 | 327(50 mA $cm^{-2}$) | [19] |
| NiMoN-550 nanotubes | 295 | 427 (207.4 mA $cm^{-2}$) | [21] |
| $Ni_2P$/$MoO_2$@$MoS_2$ | 280 | - | [22] |
| NiMoN/NF-450 | 230 | 363 | [23] |
| NiMo HNRs/TiM | 310 | - | [25] |
| Ni/$Mo_2C$-PC | 368 | - | [26] |
| Ni-Mo Ms/Cu | 335 (20 mA $cm^{-2}$) | - | [27] |
| Co/β-$Mo_2C$@N-CNTs | 356 | - | [48] |
| NF@Ni/C-600 | 265 | 353 | [49] |

**Table S6** Comparison of HER activity of Ni@NCNT/NiMoN-8 electrode with recently reported catalysts in 0.5 M $H_2SO_4$.

| **Catalysts** | **$\eta_{10}$ (mV vs RHE)** | **$\eta_{100}$ (mV vs RHE)** | **Ref.** |
|---|---|---|---|
| Ni@NCNT/NiMoN-8 | 31 | 72 | This work |
| N,P-$Mo_xC$ NF | 107 | 168(80 mA $cm^{-2}$) | [29] |
| L-$Mo_2C$ | 95.8 | - | [50] |
| mNC-$Mo_2C$@rGO-2 | 237 | - | [51] |
| $NiS_2/MoS_2$ HNW | 235 | - | [30] |
| MoP/C | 88 | - | [33] |
| CoP/NiCoP/NC | 60 | - | [34] |
| $Ni_{0.89}Co_{0.11}Se_2$ MNSN/NF | 52 | - | [38] |
| FLNPC@MoP-NC/MoP-C/CC | 74 | - | [42] |
| Co/CoP@NC | 117 | - | [43] |
| Co@N-CNTs@rGO | 87 | - | [47] |
| L-$Mo_2C$ | 170 | - | [50] |
| $MoS_2$/CNT-700 | 83 | - | [53] |

**Table S7** The relevant values of $\Delta G_{H*}$ on various catalysts.

| | Graphene | N-doped graphene | Ni(111) | Ni(111)@NC | NiMoN(101) | NC/NiMoN(101) | Pt |
|---|---|---|---|---|---|---|---|
| $\Delta G_{H*}$ (eV) | 1.24 | 0.42 | -0.62 | -0.30 | -0.13 | -0.15 | -0.11 |

# References


1 M. C. Payne, M. P. Teter, D. C. Allan, T. A. Arias, J. D. Joannopoulos, *Rev. Mod. Phys.*, 1992, **64**, 1045-1097.

2 J. P. Perdew, K. Burke, M. Ernzerhof, *Phys. Rev. Lett.*, 1996, **77**, 3865-3868

3 P. Liao, J. A. Keith, E. A. Carter, *J. Am. Chem. Soc*., 2012, **134**, 13296-13309.

4 A. Jain, G. Hautier, S. P. Ong, C. J. Moore, C. C. Fischer, K. A. Persson, G. Ceder, *Phys. Rev. B*, 2011, **84**, 045115.

5 M. Ledendecker, H. Schlott, M. Antonietti, B. Meyer, M. Shalom, *Adv. Energy Mater.*, 2017, **7**, 1601735.

6 T. Ouyang, Y. Q. Ye, C. Y. Wu, K. Xiao, Z. Q. Liu, Angew. Chem. Int. Ed., 2019, **58**, 1-7.

7 A. Wu, Y. Xie, H. Ma, C. Tian, Y. Gu, H. Yan, X. Zhang, G. Yang and H. Fu, *Nano Energy*, 2018, **44**, 353-363.

8 T. Wu, M. Pi, D. Zhang, S. Chen, *J. Power Sources*, 2016, **328**, 551-557.

9 M. K. Agusta, M. David, H. Nakanishi, H. Kasai, *Surf. Sci.*, 2010, **604**, 245-251.

10 M. K. Agusta, H. Kasai, *Surf. Sci.*, 2012, **606**, 766-771.

11 G. Prévot, D. Schmaus, S. L. Moal, *Surf. Sci.*, 2010, **604**, 770-778.

12 M. Gamil, K. Nakamura, A. M. R. Fath El-Bab, O. Tabata, A. A. El-Moneim, *Modeling and Numerical Simulation of Material Science*, 2013, **3**, 117-123.

13 L. X. Chen, Z. W. Chen, Y. Wang, C. C. Yang, Q. Jiang, *ACS Catal.*, 2018, **8**, 8107-8114.

14 X. Hu, S. Zhang, J. Sun, L. Yu, X. Qian, R. Hu, Y. Wang, H. Zhao, J. Zhu, *Nano Energy*, 2019, **56**, 109-117.

15 T. Li, G. Luo, K. Liu, X. Li, D. Sun, L. Xu, Y. Li, Y. Tang, *Adv. Funct. Mater.*, 2018, **28**, 1805828.

16 F. Wang, Y. Sun, Y. He, L. Liu, J. Xu, X. Zhao, G. Yin, L. Zhang, S. Li, Q. Mao, Y. Huang, T. Zhang, B. Liu, *Nano Energy*, 2017, **37**, 1-6.

17 J. K. Nørskov, T. Bligaard, A. Logadottir, J. R. Kitchin, J. G. Chen, S. Pandelov, U. Stimming, *J. Electrochem. Soc.*, 2005, **152**, J23.

18 L. An, J. Feng, Y. Zhang, R. Wang, H. Liu, G.-C. Wang, F. Cheng and P. Xi, *Adv. Funct. Mater.*, 2019, **29**, 1805298.

19 H. Xu, J. Wei, K. Zhang, Y. Shiraishi and Y. Du, *ACS Appl. Mater. Interfaces*, 2018, **10**, 29647-29655.

20 J. Jia, M. Zhai, J. Lv, B. Zhao, H. Du and J. Zhu, *ACS Appl. Mater. Interfaces*, 2018, **10**, 30400-30408.

21 Z. Yin, Y. Sun, C. Zhu, C. Li, X. Zhang and Y. Chen, *J. Mater. Chem. A*, 2017, **5**, 13648-13658.

22 Y. Wang, T. Williams, T. Gengenbach, B. Kong, D. Zhao, H. Wang and C. Selomulya, *Nanoscale*, 2017, **9**, 17349-17356.

23 Y. Wang, Y. Sun, F. Yan, C. Zhu, P. Gao, X. Zhang and Y. Chen, *J. Mater. Chem. A*, 2018, **6**, 8479-8487.

24 J. Tian, N. Cheng, Q. Liu, X. Sun, Y. He and A. M. Asiri, *J. Mater. Chem. A*, 2015, **3**, 20056-20059.

25 Z. Y. Yu, Y. Duan, M. R. Gao, C. C. Lang, Y. R. Zheng and S. H. Yu, *Chem. Sci.*, 2017, **8**, 968-

973.
26 M. Y. Gao, C. Yang, Q. B. Zhang, J. R. Zeng, X. T. Li, Y. X. Hua, C. Y. Xu and P. Dong, *J. Mater. Chem. A*, 2017, **5**, 5797-5805.
27 K. Li, J. Ma, X. Guan, H. He, M. Wang, G. Zhang, F. Zhang, X. Fan, W. Peng and Y. Li, *Nanoscale*, 2018, **10**, 22173-22179.
28 F. C. Shen, S. N. Sun, Z. F. Xin, S. L. Li, L. Z. Dong, Q. Huang, Y. R. Wang, J. Liu and Y. Q. Lan, *Appl. Catal. B: Environ.*, 2019, **243**, 470-480.
29 L. Ji, J. Wang, X. Teng, H. Dong, X. He and Z. Chen, *ACS Appl. Mater. Interfaces*, 2018, **10**, 14632-14640.
30 P. Kuang, T. Tong, K. Fan and J. Yu, *ACS Catal.*, 2017, **7**, 6179-6187.
31 J. Jiang, M. Gao, W. Sheng and Y. Yan, *Angew. Chem. Int. Ed.*, 2016, **55**, 15240-15245.
32 M. Fang, W. Gao, G. Dong, Z. Xia, S. Yip, Y. Qin, Y. Qu and J. C. Ho, *Nano Energy*, 2016, **27**, 247-254.
33 G. W. Li, Y. Sun, J. C. Rao, J. Q. Wu, A. Kumar, Q. N. Xu, C. G. Fu, E. K. Liu, G. R. Blake, P. Werner, B. Q. Shao, K. Liu, S. Parkin, X. J. Liu, M. Fahlman, S. C. Liou, G. Auffermann, J. Zhang, C. Felser, X. L. Feng, *Adv. Energy Mater.*, 2018, **8**, 1801258.
34 R. Boppella, J. Tan, W. Yang, J. Moon, *Adv. Funct. Mater.*, 2018, **29**, 1807976.
35 J. G. Hou, Y. Q. Sun, Z. W. Li, B. Zhang, S. Y. Cao, Y. Z. Wu, Z. M. Gao, L. C. Sun, *Adv. Funct. Mater.*, 2018, **28**, 1803278.
36 L. Yu, H. Zhou, J. Sun, F. Qin, F. Yu, J. Bao, Y. Yu, S. Chen, Z. Ren, *Energy Environ. Sci.*, 2017, **10**, 1820-1827.
37 R. Zhang, X. Wang, S. Yu, T. Wen, X. Zhu, F. Yang, X. Sun, X. Wang, W. Hu, *Adv. Mater.*, 2017, **29**, 1605502-.
38 B. Liu, Y. F. Zhao, H. Q. Peng, Z. Y. Zhang, C. K. Sit, M. F. Yuen, T. R. Zhang, C. S. Lee, W. J. Zhang, *Adv. Mater.*, 2017, **29**, 1606521.
39 Y. Luo, X. Li, X. Cai, X. Zou, F. Kang, H. M. Cheng, B. Liu, *ACS Nano*, 2018, **12**, 4565-4573.
40 Y. Wu, X. Liu, D. Han, X. Song, L. Shi, Y. Song, S. Niu, Y. Xie, J. Cai, S. Wu, J. Kang, J. Zhou, Z. Chen, X. Zheng, X. Xiao, G. Wang, *Nat. Commun.*, 2018, **9**, 1425.
41 H. Liu, X. Ma, Y. Rao, Y. Liu, J. Liu, L. Wang, M. Wu, *ACS Appl. Mater. Interfaces*, 2018, **10**, 10890-10897.
42 B. C. Liu, H. Li, B. Cao, J. N. Jiang, R. Gao, J. Zhang, *Adv. Funct. Mater.*, 2018, **28**, 1801527.
43 Y. Li, H. Li, K. Cao, T. Jin, X. Wang, H. Sun, J. Ning, Y. Wang, L. Jiao, *Energy Storage Mater.*, 2018, **12**, 44-53.
44 B. Y. Xiong, L. S. Chen, J. L. Shi, *ACS Catal.*, 2018, **8**, 3688-3707.
45 J. Zhang, Y. Li, T. Zhu, Y. Wang, J. Cui, J. Wu, H. Xu, X. Shu, Y. Qin, H. Zheng, P. M. Ajayan, Y. Zhang, Y. Wu, *ACS Appl. Mater. Interfaces*, 2018, **10**, 31330-31339.
46 M. Y. Wu, P. F. Da, T. Zhang, J. Mao, H. Liu, T. Ling, *ACS Appl. Mater. Interfaces*, 2018, **10**, 17896-17902.
47 Z. Chen, R. Wu, Y. Liu, Y. Ha, Y. Guo, D. Sun, M. Liu, F. Fang, *Adv. Mater.*, 2018, **30**, 1802011.
48 T. Ouyang, Y-Q. Ye, C-Y. Wu, K. Xiao, Z.-Q. Liu, *Angew. Chem. Int. Ed.*, 2019, **58**, 4923-4928.
49 H. Sun, Y. Lian, C. Yang, L. Xiong, P. Qi, Q. Mu, X. Zhao, J. Guo, Z. Deng, Y. Peng, *Energy Environ. Sci.*, 2018, **11**, 2363-2371.
50 W. Yuan, Q. Huang, X. Yang, Z. Cui, S. Zhu, Z. Li, S. Du, N. Qiu, Y. Liang, *ACS Appl. Mater. Interfaces*, 2018, **10**, 40500-40508.

51 D. Hou, S. Zhu, H. Tian, H. Wei, X. Feng, Y. Mai, *ACS Appl. Mater. Interfaces*, 2018, **10**, 40800-40807.

52 J. Zheng, X. L. Chen, X. Zhong, S. Q. Li, T. Z. Liu, G. L. Zhuang, X. N. Li, S. W. Deng, D. H. Mei, J. G. Wang, *Adv. Funct. Mater.*, 2017, **27**, 1704169.

53 X. Zhang, X. L. Yu, L. J. Zhang, F. Zhou, Y. Y. Liang, R. H. Wang, *Adv. Funct. Mater.*, 2018, **28**, 1706523.

54 S. Gao, Y. Zhang, Y. Zhang, B. Wang, S. Yang, *Small*, 2018, **14**, 1804388.

55 B. Liu, J. Cheng, H.-Q. Peng, D. Chen, X. Cui, D. Shen, K. Zhang, T. Jiao, M. Li, C.-S. Lee, W. Zhang, *J. Mater. Chem. A*, 2019, **7**, 775-782.

56 J. T. Ren, G. G. Yuan, C. C. Weng, L. Chen, Z. Y. Yuan, *Nanoscale*, 2018, **10**, 10620-10628.